Available online at www.sciencedirect.com
ScienceDirect
Geochimica et Cosmochimica Acta 71 (2007) 1982–1998
Geochimica et Cosmochimica Acta
www.elsevier.com/locate/gca

Abiotic formation of hydrocarbons under hydrothermal conditions: Constraints from chemical and isotope data

Qi Fu [a,*], Barbara Sherwood Lollar [b], Juske Horita [c], Georges Lacrampe-Couloume [b], William E. Seyfried Jr. [a]

[a] Department of Geology and Geophysics, University of Minnesota, Minneapolis, MN 55455, USA
[b] Stable Isotope Laboratory, University of Toronto, Toronto, Ontario, Canada M5S 3B1
[c] Chemical Sciences Division, Oak Ridge National Laboratory, Oak Ridge, TN 37831, USA

Received 15 August 2006; accepted in revised form 26 January 2007; available online 1 February 2007

Abstract

To understand reaction pathways and isotope systematics during mineral-catalyzed abiotic synthesis of hydrocarbons under hydrothermal conditions, experiments involving magnetite and CO_2 and H_2-bearing aqueous fluids were conducted at 400 °C and 500 bars. A robust technique for sample storage and transfer from experimental apparatus to stable isotope mass spectrometer provides a methodology for integration of both carbon and hydrogen isotope characterization of reactants and products generated during abiogenic synthesis experiments. Experiments were performed with and without pretreatment of magnetite to remove background carbon associated with the mineral catalyst. Prior to experiments, the abundance and carbon isotope composition of all carbon-bearing components were determined. Time-series samples of the fluid from all experiments indicated significant concentrations of dissolved CO and C_1–C_3 hydrocarbons and relatively large changes in dissolved CO_2 and H_2 concentrations, consistent with formation of additional hydrocarbon components beyond C_3. The existence of relatively high dissolved alkanes in the experiment involving non-pretreated magnetite in particular, suggests a complex catalytic process, likely involving reinforcing effects of mineral-derived carbon with newly synthesized hydrocarbons at the magnetite surface. Similar reactions may be important mechanisms for carbon reduction in chemically complex natural hydrothermal systems. In spite of evidence supporting abiotic hydrocarbon formation in all experiments, an ''isotopic reversal'' trend was not observed for ^{13}C values of dissolved alkanes with increasing carbon number. This may relate to the specific mechanism of carbon reduction and hydrocarbon chain growth under hydrothermal conditions at elevated temperatures and pressures. Over time, significant ^{13}C depletion in CH_4 suggests either depolymerization reactions occurring in addition to synthesis, or reactions between the C_1–C_3 hydrocarbons and carbon species absorbed on mineral surfaces and in solution.

1. INTRODUCTION

Hydrothermal fluids containing significant concentrations of reduced carbon species are relevant to a wide range of geochemical and geo-microbiological processes in submarine and subareal hydrothermal vent systems (Karl et al., 1980; Welhan, 1988; Charlou and Donval, 1993; Aharon, 1994; Kelley, 1996; Charlou et al., 1998; Kelley and Früh-Green, 1999; Sherwood Lollar et al., 2002, 2006; Baross et al., 2004). Indeed, the dissolved concentrations of these species in such fluids may not only provide clues to chemical and physical conditions in subsurface reaction zones, but also can fuel associated microbial communities (Deming and Baross, 1993; Karl, 1995; Kelley

* Corresponding author. Fax: +1 612 625 3819.
E-mail address: fuxx0033@umn.edu (Q. Fu).

0016-7037/$ - see front matter © 2007 Elsevier Ltd. All rights reserved.
doi:10.1016/j.gca.2007.01.022

et al., 2002, 2004). Owing to constraints imposed by a wide range of geologic and geochemical factors, abundant methane and longer chain hydrocarbons dissolved in high-temperature hydrothermal fluids issuing from vents hosted in ultramafic lithologies exposed on the Mid-Atlantic Ridge suggest abiotic formation, possibly involving Fischer–Tropsch Type (FTT) synthesis (Charlou et al., 1997, 2002; Holm and Charlou, 2001).

FTT is a common industrial process, which involves the reduction of CO molecules at elevated temperatures and variable pressures in the presence of a gas phase and transition metal-bearing catalysts to yield alkanes, alkenes, and oxygenated C containing products (Fischer and Tropsch, 1926; Kugler and Steffgen, 1979; Anderson, 1984a,b; Bell, 1986). In contrast, reduction of dissolved CO_2 (the dominant form of oxidized carbon in high-temperature hydrothermal systems) in the absence of a vapor phase has been reported in only a few experimental studies (Janecky and Seyfried, 1986; Berndt et al., 1996; Horita and Berndt, 1999; McCollom and Seewald, 2001; Foustoukos and Seyfried, 2004). Accordingly, little is known about reaction pathways by which carbon reduction reactions occur under hydrothermal conditions at elevated temperatures and pressures.

Isotopic approaches have been used as an effective tool to constrain the origin and mechanism of hydrocarbon formation in experimental and natural systems. Data suggest that thermogenic hydrocarbons become more enriched in ^{13}C with increasing molecular mass, consistent with kinetic isotope fractionation effects (Sackett, 1978; Waples and Tornheim, 1978; James, 1983; Schoell, 1983; Chung et al., 1988). Alkyl groups separating from source organic matter cleave preferentially at weaker ^{12}C–^{12}C rather than ^{12}C–^{13}C bonds, resulting in the end-products of thermal degradation being more depleted in the heavy isotope relative to the high molecular weight precursors. In contrast, earlier studies have suggested that reactions producing abiotic hydrocarbons from polymerization of methane tend to preferentially incorporate ^{12}C into longer chain hydrocarbons (Des Marais et al., 1981; Chang et al., 1983; Jenden et al., 1993; Hu et al., 1998), resulting in ethane, propane, and butane becoming increasingly depleted in ^{13}C with respect to the CH_4 precursor. More recent studies, however, have shown that such "carbon isotopic reversals" can in fact be produced in typical thermogenic hydrocarbon deposits (Du et al., 2003; Huang et al., 2004), and that even controlled experiments designed to produce hydrocarbons via abiogenic reactions do not consistently produce "inverse trends" (Hu et al., 1998; Yuen et al., 1990; McCollom and Seewald, 2006). Field studies of gases discharging from Kidd Creek in the Abitibi greenstone belt, Canada, and at other Precambrian Shield sites in Canada and South Africa have emphasized the need to incorporate carbon as well as hydrogen isotope data in order to distinguish abiogenic hydrocarbons from conventional biogenically-produced gases (Sherwood Lollar et al., 2002, 2006). To date, all these investigations have been hampered by the dearth of experimental data published for isotope fractionation during hydrocarbon-producing abiogenic reactions, such as mineral-catalyzed FTT.

2. EXPERIMENTS AND METHODS

A series of hydrothermal experiments were performed at 400 °C, 500 bar to assess chemical and isotopic changes in dissolved carbon species coexisting with magnetite, which served as a substrate for FTT synthesis. Magnetite is a ubiquitous component of ultramafic-hosted hydrothermal systems (Alt and Shanks, 2003; Seyfried et al., 2004), which underscores its use in the present series of experiments. Additionally, a slightly acidic (by addition of dilute HCl) NaCl fluid (0.5 mol/kg, pH ~ 3 to 4) was used for each experiment. The relative low fluid pH value is consistent with constraints imposed by field observations from presently active seafloor hydrothermal systems involving alteration of ultramafic lithologies (Charlou et al., 2002; Douville et al., 2002).

Magnetite for the experiments was acquired from Alfa Aesar. Grain size measurements of magnetite were conducted using laser particle size analyzer LA-920 from Horiba, which indicated an average grain size of 20 μm. 5 g magnetite and 40 g of the acidified NaCl fluid were loaded into a flexible Au/Ti reaction cell, which was placed in a steel-alloy autoclave. Time-series changes in fluid chemistry were monitored throughout the experiments using procedures described by Seyfried et al. (1987).

Three experiments were performed, each involving distinctly different sources and abundances of dissolved carbon and hydrogen. Formic acid (HCOOH) was utilized in the first experiment as the primary source of these components. At experimental conditions (400 °C, 500 bars), formic acid decomposes into equivalent amounts of CO_2 and H_2 by a decarboxylation scheme (Yu and Savage, 1998). The second and third series of experiments, however, entailed incremental injection of starting fluid with dissolved gases (H_2 and CO_2) into the reaction cell, which, in the case of experiment #3, achieved concentrations of H_2 and CO_2 similar to the first experiment after taking account of the dilution effect of the injections.

Previously, another experiment with formic acid (55 mmol/kg) was conducted in a similar experimental apparatus, but in the absence of magnetite, at bulk composition, temperature, and pressure conditions analogous to those of the present study. Results showed that the measured concentrations of CO_2 and H_2 were close to those expected for the decarboxylation of formic acid, while CO was in thermodynamic equilibrium with the H_2 and CO_2. Thus, in the absence of magnetite, the carbon mass balance is satisfied, ruling out non-conservative processes by formation of $TiCO_3$ or other carbonates.

Thermodynamic calculations using EQ3/6 and GWB software packages (Wolery and Daveler, 1992; Bethke, 1996) with an updated database (Shock et al., 1997; Sverjensky et al., 1997) generated for 400 °C, 500 bars using SUPCRT92 (Johnson et al., 1992), indicate that magnetite is the only stable mineral in the FeO–Fe_2O_3–CO_2–H_2O system at experimental conditions.

The total amount of organic carbon compounds in starting acidified NaCl fluid was determined by GE Sievers 900 Total Organic Carbon (TOC) Analyzer. Its detection limit was 0.03 parts per billion (ppb). Results showed that the

concentration of TOC in fluid source used for each experiment is 0.03 μmol/kg solution (CO_2 equivalent concentration), which was well below measured carbon levels in experiments.

Commercial and natural minerals including magnetite, often, if not always, contain background sources of carbon (McCollom and Seewald, 2001, 2003; Foustoukos and Seyfried, 2004). Accordingly, isotopic labeling techniques (99% ^{13}C) have often been relied on to assess the magnitude of carbon reduction during fluid–mineral reaction. The objectives of the present experiments preclude such an approach, since we wish to understand carbon isotope exchange as a means of constraining reaction mechanisms associated with carbon reduction processes, an objective not possible in an aqueous fluid dominated by a single carbon isotope. For this approach to achieve its goals, however, it is necessary to constrain quantitatively the abundance and isotopic composition of the magnetite-derived background carbon. This was accomplished by combustion of an aliquot of the magnetite in a sealed silica tube at 850 °C for 2 h. The amount of released CO_2 was determined manometrically and its $\delta^{13}C$ value was determined by a Finnigan MAT 252 mass spectrometer at Oak Ridge National Laboratory. These data indicate an abundance of magnetite-derived carbon of 4.9 μmol per gram magnetite with $\delta^{13}C$ of $-12.8‰$ (V-PDB). A similar concentration (4.6 μmol per gram magnetite) of magnetite-derived carbon was also determined by digestion of the magnetite in aqua regia followed by measurement of the evolved CO_2 by gas chromatography.

In addition to different sources of dissolved carbon (formic acid, direct gas injection), the experiments differed in the preconditioning of the magnetite catalyst. For example, Experiment #1 involved untreated magnetite, and thus, background carbon sources could participate in the reaction. In contrast, the magnetite used for Experiments #2 and #3 was pretreated with hydrogen peroxide to eliminate organic species chemisorbed on the magnetite surface. Subsequently, the magnetite was kept in an anaerobic environment prior to transfer to the reaction cell, which had been similarly pretreated with aqua regia to remove potential carbon contaminants. The only difference between Experiments #2 and #3 involved the concentrations of the inorganically derived dissolved CO_2 and H_2. As noted, the relatively high dissolved CO_2 and H_2 concentrations for Experiment #3 were used to provide a comparison with the high values of these species achieved in Experiment #1 from formic acid decarboxylation. Finally, comparison of results of Experiments #1 and #3 provide some insight on the potential role of surface carbon species as an additional catalyzing agent for carbon reduction, when subjected to hydrothermal alteration processes.

To evaluate the abundance and composition of dissolved carbon species that could be released from untreated magnetite and pretreated magnetite, two "control" experiments were preformed. Both experiments involved hydrothermal annealing of previously untreated (control Experiment 1c) and treated (control Experiment 2c) magnetite, respectively, in an acidified NaCl fluid, keeping temperature, pressure, and the mineral/fluid ratio identical to the actual experiments, while monitoring concentrations of the dominant dissolved carbon species. In control Experiment 2c, dissolved H_2 concentration increased due to incremental addition of H_2-charged fluid.

A Perkin-Elmer Auto-system gas chromatograph (GC), which houses a 30-m, 0.53-mm (ID) fused silica capillary column (Carboxen 1010 PLOT) (Supelco), was used to analyze dissolved gas components in fluid samples. Temperature programmed step-heating was performed as follows: 40 °C for 1.7 min, 40 °C/min to 220 °C, 220 °C for 20 min. Argon was the carrier gas at a flow rate of 20 ml/min. Two detectors were used for gas analysis: flame ionization detector (FID) for carbon-bearing species, and thermal conductivity detector (TCD) for H_2. The detection limit of hydrocarbons is 1 μmol/kg. Uncertainties in reported concentrations are estimated to be within ±5%.

The paucity of published results to date on fractionation factors associated with abiogenic hydrocarbon formation processes is directly related to two challenges: (1) obtaining $\delta^{13}C$ and $\delta^{2}H$ values on the small volumes of material typically produced in abiogenic hydrocarbon synthesis experiments; and (2) sample transfer from the experimental apparatus to a stable isotope ratio mass spectrometer. While $\delta^{13}C$ values have been obtained for abiogenically synthesized hydrocarbons in a few recent studies (Horita and Berndt, 1999; McCollom and Seewald, 2006), the dataset is limited and no $\delta^{2}H$ values have yet been published from such experiments. To address this gap, the current study developed a practical and robust method to couple the experimental and analytical aspects of this challenge. Carbon and hydrogen isotope analyses of the gas samples were conducted at the Stable Isotope Laboratory, University of Toronto. In anticipation of this, fluid samples were withdrawn from the hydrothermal reactor at University of Minnesota by action of a high-pressure sampling valve, which diverted the fluid into preweighed glass gas-tight syringes. Gas components in the headspace were then transferred to sampling vials, which had been previously evacuated. The sample vials permitted storage of the samples, prior to transfer to the University of Toronto. These 7 ml borosilicate vials sealed with blue butyl rubber stopper and aluminum crimp seals have been extensively tested for sample storage and analysis (Ward, 2002; Ward et al., 2004). All stoppers were pretreated by boiling in 0.1 mol/l NaOH for an hour as per accepted practice (Oremland and Des Marais, 1983). During the entire sampling and transfer process, the samples were overpressurized with respect to ambient conditions by injecting gas into the sampling vials to approximately 30% more than the vial capacity to inhibit fractionation effects. This slight overpressurization has been shown to be an important step to eliminate fractionation effects associated with depressurizing the vials as aliquots are successively withdrawn for analysis (Ward, 2002).

As an additional quality control step to verify the approach described above, a series of initial experiments were run in which isotopically characterized laboratory working standards of H_2, CH_4, C_2H_6, C_3H_8, CO_2 and CO with known isotopic compositions were mixed in the same ratios as the samples, input into the sampling vials in the same concentrations and run by the same GC methods. As dem-

onstrated in Table 1, in all cases, the $\delta^{13}C$ and $\delta^{2}H$ values obtained in these protocol tests were within uncertainty of the known isotopic values for the standards. This is an important result that validates and establishes a robust protocol that should be a useful step in advancing the number of abiogenic synthesis experiments for which isotopic characterization of the reactants and products can be integrated, and to address the gap in the known carbon and hydrogen isotope fractionation factors for abiogenic reactions.

Carbon isotope analyses were conducted on a GC-C-IRMS system composed of a Varian 3400 capillary gas chromatograph, and an oxidation oven at 980 °C interfaced directly to a Finnigan 252 gas source mass spectrometer. To separate CO and CH_4, a 30 m Molecular Sieve column (0.32 mm ID) was used. The temperature program started at 40 °C (hold 2 min), ramped to 180 °C at 10 °C per minute and ramped to 230 at 20 °C per minute (hold 10 min). CO_2, C_2H_6, and C_3H_8 were analyzed on a 30 m Poraplot U column (0.32 mm ID). The temperature program started at 30 °C (hold 12 min), ramped to 60 °C at 5 °C per minute and ramped to 185 °C at 15 °C per minute (hold 2 min). All samples were run in duplicate and mean values were reported. Reproducibility was typically ±0.2‰ to 0.3‰ but total uncertainty, incorporating both accuracy and reproducibility was ±0.5‰ with respect to V-PDB standard as per Ward et al. (2004).

Hydrogen isotope analyses were conducted on a GC-TC-IRMS system composed of an Agilent G1530A capillary gas chromatogram, a pyrolysis oven at 1440 °C and a Finnigan Delta XL gas source mass spectrometer. H_2 and CH_4 were separated on a 30 m Molecular Sieve column (0.32 mm ID). The temperature program started at 40 °C (hold 5 min), ramped to 180 °C at 10 °C per minute and ramped to 230 °C at 20 °C per minute (hold 10 min). C_2H_6 and C_3H_8 were analyzed on a 25 m GSQ column (0.32 mm ID). The temperature program started at 30 °C (hold 3 min), ramped to 185 °C at 7 °C per minute (hold 2 min). All samples were run in duplicate and mean values were reported. Reproducibility was typically ±2‰ to 3‰ but total uncertainty, incorporating both accuracy and reproducibility is ±5‰ with respect to V-SMOW standard as per Ward et al. (2004).

The $\delta^{13}C$ value of formic acid, which was used as the carbon source in Experiments #1, was measured at Oak Ridge National Laboratory. About 4 mg of the starting formic acid was sealed and heated in a Pyrex tube at 400 °C over night. The CO_2 converted was purified, and its $^{13}C/^{12}C$ ratio was determined with Finnigan MAT 252 isotope ratio mass spectrometer.

X-ray photoelectron spectroscopy (XPS) was used to determine structural states of carbon species on the surface of the magnetite catalyst following experiments. The XPS spectra were collected on a Physical Electronics 5400. Non-monochromatic Mg Kα radiation operated at 300 W served as the X-ray source. Each powder sample was embedded on double-sided adhesive tape, which was then fixed on the sample holder. The samples were degassed in the introduction chamber to 10^{-7} Torr before entering the main chamber, in which the vacuum was kept at 5×10^{-8} Torr during data acquisition. The area of analysis was 1 by 1.414 mm, while the photoelectron take-off angle was 45°. Survey scans (0–1100 eV binding energy) were performed first to determine the near-surface composition of the samples, followed by multiplex repetitive scans over the C 1s energy region. Multiplet fittings of C 1s spectra by the Gaussian–Lorentzian method were carried out to determine the atomic environment of C in all samples.

Magnetite was analyzed by X-ray diffraction (XRD) before and after experiments, with a Siemens D-5005 diffractometer using sealed copper X-ray source. Accelerating voltage and current were set to be 45 kV and 40 mA, respectively. System calibration was conducted with quartz standard at the beginning of each scan session. Scanning angle (2θ) ranged from 20° to 120°, with scan step of 0.02° and dwell time of 1.0 s. Powder samples were loaded in rectangular plexiglass top-pack holders. Data analysis and phase identification were performed with Jade program using PDF-4 database from International Centre for Diffraction Data (ICDD).

3. RESULTS

3.1. Fluid chemistry

Results from the control Experiment 1c reveal that dissolved CO_2 and CH_4 are the dominant carbon species released from magnetite during hydrothermal annealing (Table 2). The $CO_{2(aq)}/CH_{4(aq)}$ ratio rapidly achieved a steady state value of approximately 4, likely indicating source limitation (Table 2). For example, as noted previously, combustion and quantitative extraction of total carbon from the untreated magnetite indicated 4.9 μmol carbon per gram magnetite. Since all experiments performed as part of the present investigation used 5 g magnetite and 40 g fluid, the total carbon available to the fluid from the

Table 1
Comparison of sample protocol tests using isotopically characterized laboratory working standards with known standard values

	$\delta^{13}C$ values (‰)					$\delta^{2}H$ values (‰)			
	CO_2	CO	CH_4	C_2H_6	C_3H_8	H_2	CH_4	C_2H_6	C_3H_8
Protocols[a]	−42.4	−38.1	−18.4	−31.7	−32.7	−751	−101	−116	−136
N	6	6	12	13	14	6	6	16	17
Known values	−43.0	−38.3	−18.0	−31.7	−32.6	−756	−101	−120	−145

N, number of protocol test runs.
[a] Protocol $\delta^{13}C$ values are reported as the mean of the test runs (*N*).

Table 2
Chemical and isotopic compositions of dissolved aqueous species during hydrothermal carbon reduction processes

Time (h)	Chemical composition (mmol/kg)							Isotopic composition (‰)											
	H_2	CO_2	CO	CH_4	C_2H_6	C_3H_8	C_S[b]	$\delta^{13}C_{CO_2}$	$\delta^{13}C_{CO}$	$\delta^{13}C_{C_1}$	$\delta^{13}C_{C_2}$	$\delta^{13}C_{C_3}$	$\delta^{13}C_{C_4}$	$\delta^{13}C_{C_s}$[c]	$\delta^{2}H_{C_1}$	$\delta^{2}H_{C_2}$	$\delta^{2}H_{C_3}$	$\delta^{2}H_{H_2}$	$\delta^{2}H_{H_2O}$[e]
Control Experiment 1c																			
48	0.26	0.47	*b.d.*[a].	0.12	*b.d.*	*b.d.*													
144	0.28	0.46	*b.d.*	0.12	*b.d.*	*b.d.*													
Control Experiment 2c																			
168	*b.d.*	*b.d.*	*b.d.*	*b.d.*	*b.d.*	*b.d.*													
192	Injection of H_2-charged fluid																		
360	0.20	*b.d.*	*b.d.*	*b.d.*	*b.d.*	*b.d.*													
384	Injection of H_2-charged fluid																		
744	22	*b.d.*	*b.d.*	*b.d.*	*b.d.*	*b.d.*													
Experiment #1[d]																			
66	121	140.6	0.74	0.39	0.04	*b.d.*		−31.5	−49.3	−36.1	−31.1	−30.5	−25.9		−253	−276	−248	−372	−74
570	128	143.2	0.83	0.63	0.09	*b.d.*	9.5	−31.6	−48.4	−46.3	−30.2	−28.9	−24.5	−23.8	−262	−288	−243	−376	−86
Experiment #2																			
0	0.07	*b.d.*	*b.d.*	*b.d.*	*b.d.*	*b.d.*													
6	Injection of CO_2-charged fluid																		
25	0.07	59.0	*b.d.*	*b.d.*	*b.d.*	*b.d.*													
46	Injection of H_2-charged fluid																		
70	25	52.4	0.06	0.01	*b.d.*	*b.d.*													
94	Injection of H_2-charged fluid																		
170	45	50.6	0.09	0.07	*b.d.*	*b.d.*													
192	Injection of H_2-charged fluid																		
270	55	47.3	0.12	0.09	*b.d.*	*b.d.*													
294	Injection of H_2-charged fluid																		
846	72	46.3	0.13	0.13	0.01	0.01	13.1	−12.5	−31.4	−28.5	−23.4	−23.8	*b.d.*	−27.7	−269		−234	−377	−81
Experiment #3																			
0	0.09	*b.d.*	*b.d.*	*b.d.*	*b.d.*	*b.d.*													
24	Injection of CO_2-charged fluid																		
68	0.08	138.6	*b.d.*	*b.d.*	*b.d.*	*b.d.*													
92	Injection of H_2-charged fluid																		
270	52	131.6	0.29	0.01	*b.d.*	*b.d.*													
318	Injection of H_2-charged fluid																		
510	150	125.0	0.90	0.31	0.02	0.02		−11.9	−33.6	−33.5	−28.0	−25.7	*b.d.*		−268			−385	
1015	150	123.2	0.85	0.32	0.02	0.02	3.7	−12.1	−31.3	−39.2	−25.8	−23.7	*b.d.*	−23.2	−268			−383	

The C and H isotope values of formic acid in Experiment 1 are: $\delta^{13}C = -29.8‰$, $\delta^{2}H = -85‰$. The isotope values of CO_2 and H_2 source in Experiments 2 and 3 are: $\delta^{13}C_{CO_2} = -12.2‰$, $\delta^{2}H_{H_2} = -192‰$. In Experiments #2 and #3, time zero was set after injecting sufficient H_2 into the reaction cell to restore the magnetite structure. The detection limit of dissolved aqueous species is 1 μmol/kg. The overall analytical error for concentration measurements is ±5%. Errors for C and H isotope analysis are ±0.5‰ and ±5‰, respectively. Dilution effects were taken into account in experiments involving injection of gas-charged fluid. Fluid composition analysis indicated the formic acid was under detection limit in all experiments.

[a] *b.d.*: below detection limit.

[b] Concentration of carbon species on magnetite surface after each experiment, in μmol carbon per gram magnetite.

[c] Measured C isotope value of carbon species on magnetite surface after each experiment. Only in Experiment #1, starting magnetite contained carbon species (0.6 mmol/kg) on its surface with a $\delta^{13}C$ value of −12.8‰.

[d] In Experiment #1, the concentrations of CO_2 and H_2 were expected to be 170 mmol/kg, owing to decarboxylation of formic acid.

[e] $\delta^{2}H$ values of H_2O in starting NaCl fluid in Experiments #1 and #2 are −79‰ and −82‰, respectively.

background source is approximately 0.6 mmol/kg. This is in excellent agreement with the sum of dissolved CO_2 and CH_4 actually observed in the control Experiment 1c (Table 2), supporting our interpretation of rapid and quantitative release of the magnetite-derived carbon during the experiment.

In the first non-control experiment (Experiment #1), in which formic acid was used as the carbon source, CO, CH_4 and C_2H_6 were detected as reduced carbon species (Table 2 and Fig. 1). Based on the abundance of formic acid added, H_2 and CO_2 concentrations of 170 mmol/kg were predicted. Instead, there was $40 \sim 50$ mmol/kg less H_2 and 30 mmol/kg less CO_2, suggesting formation of other hydrocarbon components, perhaps directly associated with the surface of the magnetite catalyst and/or dissolved in solution (Table 2). After 570 h of reaction, concentrations of dissolved CO and CH_4 increased significantly, reaching 0.83 and 0.63 mmol/kg, respectively, accompanied by formation of 0.09 mmol/kg C_2H_6. Quantitative analysis of the magnetite surface after the experiment indicated the abundance of surface carbon increased from 4.9 to 9.5 μmol carbon per gram magnetite, which corresponds to CO_2 equivalent concentration of 1.2 mmol/kg (Table 2).

In control Experiment 2c for pre-treated magnetite, no carbon-bearing species were detected with incremental increases of dissolved H_2 (Table 2), confirming the effectiveness of removal of background carbon sources by the magnetite pretreatment process. Therefore, the results of Experiments #2 and #3 (pre-treated magnetite and incremental additions of inorganically-sourced CO_2 and H_2) contrast with those of Experiment #1. In particular, the absence of surface carbon components on magnetite results in an initial condition in which the fluid lacks reduced dissolved carbon species. Moreover, the relatively low dissolved H_2 concentration condition during the incipient stage of reaction (Table 2) places the fluid in the magnetite field of stability, but very close to the hematite–magnetite join. Subsequent addition of dissolved CO_2 to Experiments #2 and #3 resulted in approximately 59 and 139 mmol/kg CO_2, respectively (Table 2 and Fig. 1). There were no changes in dissolved carbon species, however, until H_2 was added, also by injection of the dissolved gas. The incremental increase in dissolved H_2 caused an immediate and significant increase in the dissolved concentration of CO, CH_4, C_2H_6 and C_3H_8 (C_1–C_3 hydrocarbons), while the concentration of CO_2 decreased (Table 2 and Fig. 1). The concentrations of surface carbon species on retrieved magnetite after Experiments #2 and #3, were 13.1 and 3.7 μmol carbon per gram magnetite, respectively (Table 2). This indicated an abundance of surface carbon of 1.6 mmol/kg in Experiment #2, and 0.4 mmol/kg in Experiment #3. As with Experiment #1, the decrease in dissolved CO_2 is considerably greater than can be accounted for by the formation of surface carbon species and dissolved reduced carbon species detected in the fluids, indicating the presence of other reduced carbon-bearing components in the aqueous phase.

Thermodynamic calculations indicated that, in all three experiments, CO_2 and CO achieved chemical equilibrium via the reaction $CO_2 + H_2 = CO + H_2O$. The amounts of C_1–C_3 hydrocarbons, however, were much less than theoretical predictions. The concentration of CH_4 was always considerably in excess of C_2H_6 and C_3H_8. This might indicate that the bulk properties of the catalyst (magnetite/hydrocarbon), together with constraints imposed by chemical and physical conditions, facilitate methane formation mechanisms.

3.2. Carbon isotope data

Equilibrium carbon isotope fractionation in the system C–O–H, including CO, CO_2, CH_4 and other light hydrocarbons, are reasonably well understood based on several theoretical and experimental studies (see Fig. 1 of Horita, 2005 for a summary). CO is most depleted in ^{13}C, followed by CH_4, while CO_2 is most enriched in ^{13}C. Among light hydrocarbons (C_1–C_4), $\delta^{13}C$ values slightly increase with increasing carbon numbers (Galimov, 1975). These data are all for gaseous species, but the magnitude of fractionation between gaseous and dissolved species is most likely small (<1‰) (Horita and Cole, 2004; Horita, 2005). The aqueous CO_2 species in our experiments are dominated by CO_2(aq), rather than HCO_3^- or CO_3^{2-}.

Carbon isotope analysis performed on CO_2, CO, and dissolved hydrocarbons produced in all three experiments (Table 2) shows that the $\delta^{13}C$ value of formic acid used for Experiment #1 was −29.8‰, but CO_2 derived from decarboxylation of formic acid was 1.8‰ lighter in ^{13}C than this source. The general pattern of $\delta^{13}C$ values among CO_2, CO and CH_4 is consistent with their equilibrium pattern ($CO_2 > CH_4 > CO$) (Fig. 2). However, the magnitudes of their fractionations are smaller than corresponding values based on theoretically predicted isotopic equilibrium constraints (Table 3). For example, assuming carbon isotopic equilibrium at 400 °C, CO_2 should be 18.5–19‰ enriched in ^{13}C relative to CH_4, and 23‰ enriched in ^{13}C relative to CO (Richet et al., 1977; Horita, 2001). Thus, the experimental results showed that the carbon isotope fractionation between CO_2 and CO was 16.8–17.8‰, which is approximately 6‰ less than the corresponding equilibrium value. The $\delta^{13}C$ values between CO_2 and CH_4 varied from 4.6‰ to 14.7‰, the latter value being largely influenced by the conspicuous decrease (10.2‰) in ^{13}C of CH_4 after 570 h of reaction (Table 2 and Fig. 2).

The $\delta^{13}C$ values of C_1-C_4 hydrocarbons from Experiment #1 were measured at 66 and 570 h of reaction (Table 2 and Fig. 3). Although C_3H_8 and C_4H_{10} were not detected in the fluid by GC analysis, mass spectrometry was sufficiently sensitive that isotope data could still be determined. In general, at 66 h of reaction, $\delta^{13}C$ of CH_4 was 5‰ less than that of C_2H_6, which increased to 16.1‰ after 570 h (Table 2). Moreover, $\delta^{13}C$ of C_2H_6 was 0.9 ± 0.4‰ less than C_3H_8, and C_3H_8 was 4.5 ± 0.1‰ less than C_4H_{10}. Overall, the observed $\delta^{13}C$ values of C_1–C_4 hydrocarbons increased with carbon number, which is consistent with their equilibrium pattern, but the differences between C_2H_6, C_3H_8, C_4H_{10} and CH_4 are higher than corresponding equilibrium values, respectively (Table 3). Furthermore, the $\delta^{13}C$ values of C_2–C_4 are slightly greater than that of CO_2, which is not in accord with equilibrium distribution. The

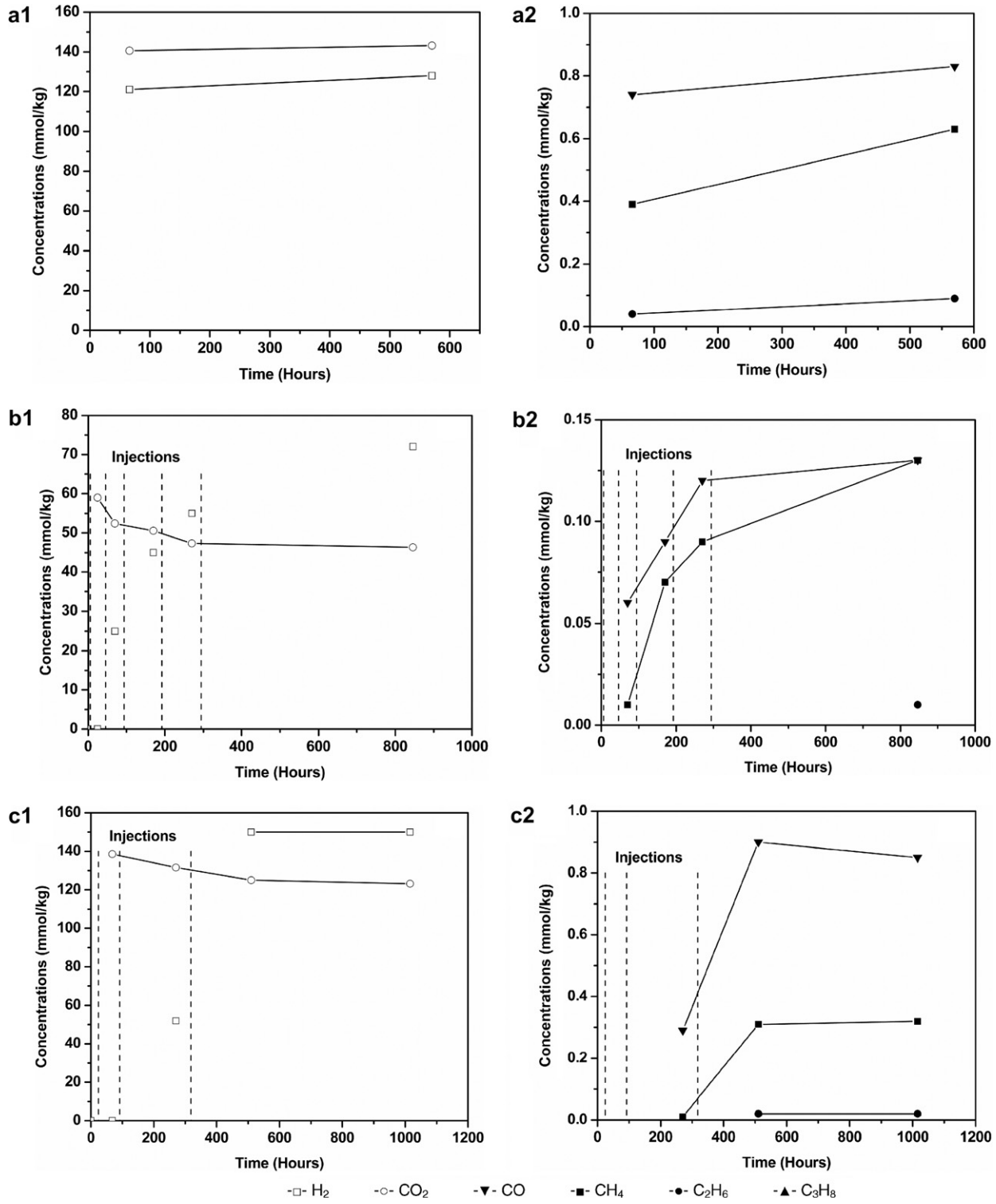

Fig. 1. Measured concentrations of dissolved H_2, CO_2 and reduced carbon species (including CO, CH_4, C_2H_6 and C_3H_8) as a function of time in three hydrothermal experiments involving carbon reduction processes at 400 °C and 500 bars. (a) Experiment #1 with formic acid as carbon precursor (a1 and a2); (b) Experiment #2 with CO_2 gas as carbon precursor at low carbon concentrations (b1 and b2); (c) Experiment #3 with CO_2 gas as carbon precursor at high carbon concentrations (c1 and c2). Dashed lines indicate injections of CO_2- or H_2-charged fluid (see text and Table 2).

conspicuous decrease in $\delta^{13}C$ of C_1 at 570 h is particularly noteworthy in comparison with the increase in all other reduced carbon species (Table 2 and Fig. 2), suggesting a causative relationship (see below).

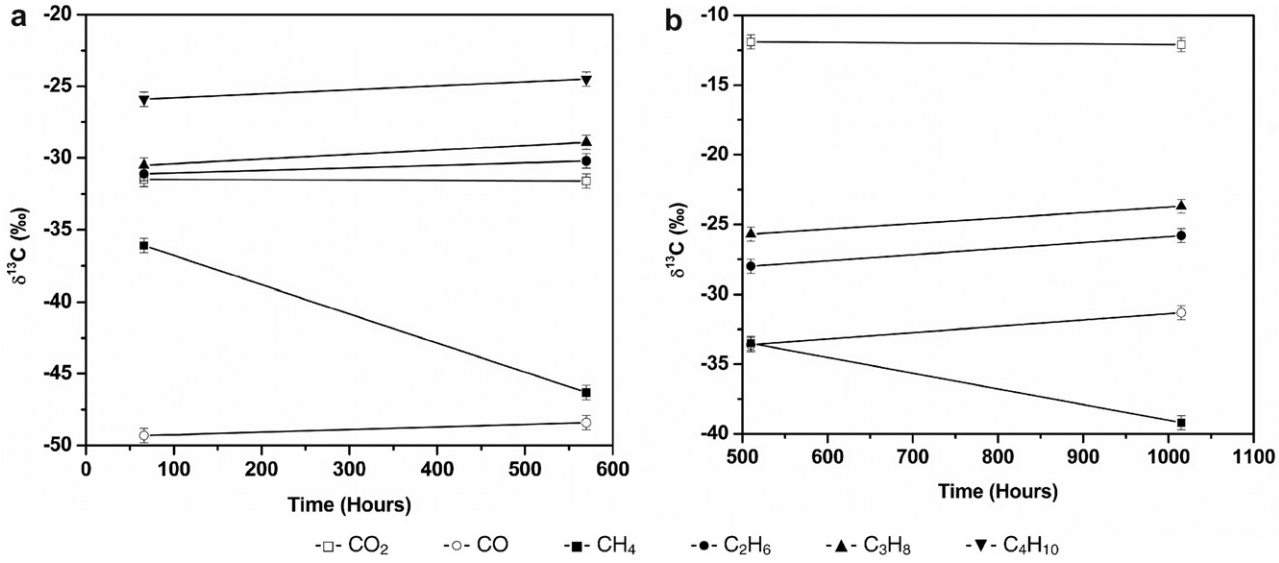

Fig. 2. Time-series $\delta^{13}C$ values of hydrocarbon species (C_1–C_4) derived from hydrothermal experiments at 400 °C and 500 bars. (a) Experiment #1 with formic acid as carbon precursor; (b) Experiment #3 with CO_2 gas as carbon precursor at high carbon concentrations. Error bars are ±0.5‰. In both experiments, the $\delta^{13}C$ values of CO, C_2H_6 and C_3H_8 increased, and CH_4 decreased with progress of the reaction. The carbon isotope of CO_2 remained constant.

Table 3
Comparison of calculated isotope fractionation values (1000 ln α) for species pairs to corresponding theoretical equilibrium fractionation values at 400 °C (Galimov, 1975; Richet et al., 1977; Horibe and Craig, 1995; Horita, 2001)

	$^{13}C/^{12}C$					D/H		
	CO_2–CO	CO_2–CH_4	C_2H_6–CH_4	C_3H_8–CH_4	C_4H_{10}–CH_4	H_2O–CH_4[a]	H_2O–H_2[a]	CH_4–H_2
Equilibrium	23	19	2	3	4	132	398	266
Experiment #1								
66 h	17.8	4.6	5	5.6	10.2	214	388	174
570 h	16.8	14.7	16.1	17.4	21.8	214	381	168
Experiment #2								
846 h	18.9	16	5.1	4.7		229	389	160
Experiment #3								
510 h	21.7	21.6	5.5	7.8		228	402	174
1015 h	19.2	27.1	13.4	15.5		214	398	184

[a] For Experiment #3, calculation is based on average δ^2H value for water of −81‰ from Experiments #1 and #2 (see Table 2).

Analysis results from Experiment #2 indicate a $\delta^{13}C$ value of dissolved CO_2 gas of −12.2‰, in sharp contrast with the formic acid derived $\delta^{13}C$ value observed in Experiment #1 (Table 2). Moreover, there was essentially no change in $\delta^{13}C$ of CO_2 after more than 800 h of reaction. The $\delta^{13}C$ difference between CO_2 and CH_4 was 3‰ less enriched in the heavier isotope than the equilibrium fractionation value of 18.5–19‰ at 400 °C (Table 3). Among hydrocarbons, CH_4 is approximately 5‰ less enriched in ^{13}C than C_2H_6 and C_3H_8, both of which have identical $\delta^{13}C$ values (Table 2 and Fig. 3). Overall, the $\delta^{13}C$ values of CO_2, C_1–C_3 hydrocarbons are closer to their equilibrium distribution compared to those of Experiment #1 (Table 3).

The dissolved CO_2 gas source for Experiment #3 was the same as Experiment #2, although the dissolved concentration was considerably greater than Experiment #2, more in keeping with Experiment #1, as noted earlier. Owing to mass balance constraints, therefore, the apparent lack of change in $\delta^{13}C$ of CO_2 during the experiment is not surprising. $\delta^{13}C$ values of dissolved CO, which are 20.9 to 22.2‰ lighter than those of CO_2 at 510 and 1015 h, respectively, appear to approach that of an equilibrium value (22.9‰ lighter) with CO_2. The difference in $\delta^{13}C$ between CO_2 and CH_4 (24.4 ± 2.8‰), however, is distinctly higher than the predicted equilibrium value (Table 3). As with results from Experiment #1, $\delta^{13}C$ values of C_1–C_3 hydrocarbons increased with carbon number, while there was also a noteworthy decrease in $\delta^{13}C$ value of CH_4 with reaction progress, which was not reflected in the isotopic composition of the other reduced dissolved carbon species (Table 2 and Fig. 2).

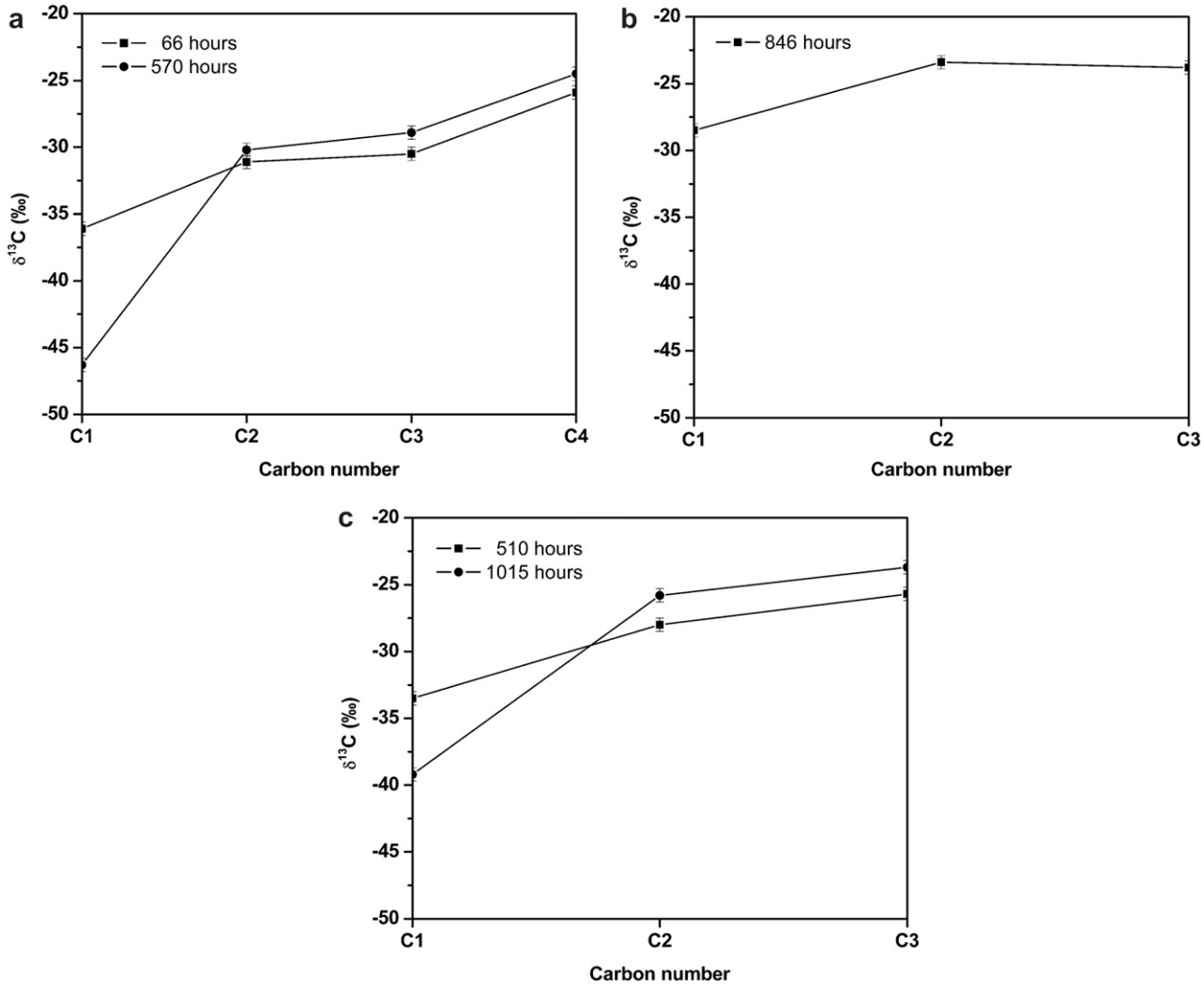

Fig. 3. $\delta^{13}C$ values of hydrocarbon species (C_1–C_4) with carbon numbers, which were derived from three hydrothermal experiments involving carbon reduction processes at 400 °C and 500 bars. (a) Experiment #1 with formic acid as carbon precursor; (b) Experiment #2 with CO_2 gas as carbon precursor at low carbon concentrations; (c) Experiment #3 with CO_2 gas as carbon precursor at high carbon concentrations. Error bars are ±0.5‰. In all of three experiments, the $\delta^{13}C$ values of C_1–C_4 hydrocarbons keep increasing with carbon numbers.

To better constrain carbon isotope systematics in the series of hydrothermal experiment reported here, carbon isotope analysis was also determined for the surface carbon associated with the untreated magnetite and magnetite products. These data indicate an initial $\delta^{13}C$ value of −12.8‰ prior to reaction, but a considerably lower value of −23.8‰ following the Experiment #1. In Experiments #2 and #3 with pretreated magnetite, the $\delta^{13}C$ values of surface carbon species are −27.7‰ and −23.2‰, respectively, following the reactions.

3.3. Hydrogen isotope data

We also have conducted hydrogen isotope analysis of H_2 and C_1–C_3 hydrocarbons, perhaps one of the first such studies. δ^2H values of the initial water and H_2 are about −80‰ and −192‰, respectively. The former value is expected to stay constant during our experiments because of its overwhelming large reservoir compared to other H-bearing species.

In contrast to carbon isotope results, δ^2H isotope values are highly uniform not only over time but from one experiment to the next (Table 2). For instance, all five samples measured for dissolved H_2 in Experiments #1–#3 are within uncertainty of each other (the average δ^2H value of -379 ± 5‰). The same invariance is seen for CH_4. All five samples from the three experiments are within uncertainty of the average δ^2H value of -264 ± 7‰. For C_2 and C_3 hydrocarbons, most of the samples were below detection for δ^2H analysis, but for the two values of δ^2H analyzed for ethane in Experiment #1, and for the three values for propane in Experiments #1 and #2, once again the values show very little variability (Table 2).

Based on a theoretical isotopic equilibrium value for $1000\ln\alpha$ for H_2O–H_2 of 398 at 400 °C (Richet et al., 1977; Horibe and Craig, 1995), the δ^2H values for the H_2O–H_2 system have achieved isotopic equilibrium (Table 3). This is not surprising given the well-established rapid rate of equilibration between these two species. In contrast,

Table 3 shows that calculated equilibration values of $1000\ln\alpha$ for the pairs H_2O–CH_4 and CH_4–H_2 are not consistent with the expected values based on maximum theoretical equilibration at 400 °C. Nonetheless, it is important to note that the calculated $1000\ln\alpha$ values based on the δ^2H data are constant in all three experiments and fall in a very narrow range of 214–229 and 160–184 for H_2O–CH_4 and CH_4–H_2, respectively (Table 3). If a given system is not at all controlled by equilibration, a large variation in calculated values for $1000\ln\alpha$ is typically observed (see values for the CO_2–CH_4 pair in Table 3). The relatively narrow range and constant values observed for H_2O–CH_4 and CH_4–H_2 suggest that despite the differences in experimental design, a significant controlling parameter constrained δ^2H values for all three species. While inconsistent with complete isotopic equilibrium except for H_2O–H_2, the data suggest partial equilibration for H_2O–CH_4 and CH_4–H_2 may have been attained. The measured δ^2H values for CH_4 are dominated by the much larger H_2 and H_2O phases.

3.4. XPS and XRD data

As emphasized above, the surface of the untreated magnetite contained approximately 4.9 μmol carbon per gram magnetite that was likely introduced in the manufacturing process. Analysis of magnetite by mass spectrometry following Experiment #1, however, indicated a greater value (9.5 μmol per gram magnetite). There also are 13.1 and 3.7 μmol surface carbon per gram magnetite following Experiment #2 and #3, respectively, suggesting carbon enrichment on magnetite during the experiments. Formation of surface carbon-bearing phases on magnetite and formation of coexisting aqueous hydrocarbons can also be inferred from time-series changes involving dissolved CO_2 and H_2 during Experiments #1, #2 and #3 (Table 2). To better understand the implications of carbon enrichment on magnetite reactants, however, magnetite retrieved from each experiment was examined by X-ray photoelectron spectroscopy (XPS). Results show that magnetite from all three experiments has the same C 1s line shapes, but rather different normalized peak areas. These data suggest that there were different abundances of surface carbon phase(s) resulting from each experiment, which is not surprising considering constraints imposed by pretreatment processes and the distinctly different concentrations of dissolved carbon and hydrogen, and reaction times, characterizing each experiment. Data for magnetite from Experiment #2 illustrate the usefulness of XPS as a means of constraining the nature of carbon compounds on the mineral surface (Fig. 4). For example, by curve fitting these data, it can be seen that three peaks characterize the carbon-bearing species on magnetite. The main peak is at 285.0 eV, reflecting functional groups containing C–C or C–H bonds. These could be basic hydrocarbon units, such as alkyl (CH_3–CH_2-) or methylene (-CH_2-) groups, or other long chain hydrocarbons formed in experiments. Two other peaks with relatively small areas at 286.6 and 288.7 eV, can be attributed to alcohol groups (C–OH) and carboxyl groups (–COOH), respectively.

XRD results showed the coexistence of magnetite and a trivial amount of hematite before hydrothermal reaction. The existence of trace hematite is considered to be due to oxidation during sample preparation. Magnetite was the only phase recognized by XRD after reaction. Neither XRD nor XPS data indicate carbide groups or graphite formation during experiments.

4. DISCUSSION

4.1. Fluid chemistry and carbon reduction processes

All three experiments involving carbon reduction processes shared two common characteristics: (1) chemical equilibrium between dissolved CO_2, CO and H_2, in general agreement with results of other hydrothermal experiments involving the CO_2–H_2O–H_2 system at elevated temperatures and pressures (Seewald et al., 2006); and, (2) an apparent, yet complex, relationship between carbon reduction processes and dissolved $H_{2(aq)}/CO_{2(aq)}$ ratio. With specific reference to the latter observation, data indicate that when $H_{2(aq)}/CO_{2(aq)}$ ratio is relatively low, there is limited formation of reduced carbon species. When the ratio is increased by direct injection of dissolved H_2, as in Experiments #2 and #3, however, corresponding increases in dissolved CO and coexisting hydrocarbons are evident. On the other hand, a more complex relationship between $H_{2(aq)}/CO_{2(aq)}$ ratio and coexisting dissolved concentrations of reduced carbon species is manifested by results from Experiment #1. In this case, a relatively low ratio (~0.9–1.0) is associated with dissolved hydrocarbons of unusually high concentrations, indicating that other factors, perhaps involving absolute concentrations of dissolved H_2 and CO_2, or more complex catalytic effects, including long chain hydrocarbons on the magnetite surface, may be more important. Mass balance constraints involving phase relations in the CO_2–H_2O–H_2 system, however, may help to account for this apparent irregularity.

Results from the control Experiment 1c confirm the existence of carbon-bearing compounds chemisorbed on magnetite surfaces and their subsequent release to solution during hydrothermal alteration. Data indicate that the hydrothermal breakdown of surface carbon results in increases in dissolved CO_2 and CH_4. Thus, in Experiment #1 (non-treated magnetite), the formation of CH_4 and other hydrocarbons might involve three different reaction pathways: (1) direct decomposition of magnetite-derived surface carbon compounds; (2) subsequent reduction of CO_2 from surface carbon compounds by FTT synthesis; and (3) reduction of formic acid-derived CO_2 by FTT synthesis. In Experiment #3, in contrast, the only source of dissolved CO_2 for FTT synthesis was that initially injected into the fluid in the reaction cell. Although formation of hydrocarbons, such as CH_4, definitely occurred due to simple decomposition of surface carbon compounds during Experiment #1, the concentrations of dissolved reduced carbon species are clearly in excess of those possible by the known abundance of the "background carbon", strongly suggesting FTT synthesis as well (see below). Moreover, comparison of results of Experiments #1 and #3, indicate

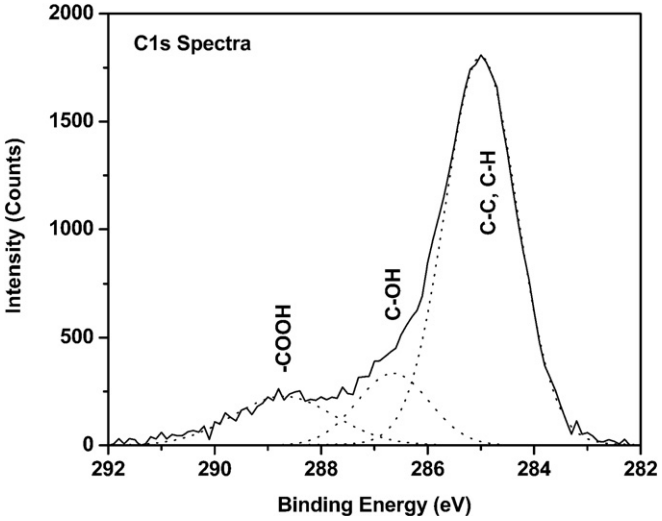

Fig. 4. XPS spectra obtained for C 1s (solid line) on magnetite surfaces following experiments. Results from all of three experiments have same C 1s line shapes, but different normalized peak areas because of different carbon levels. Only XPS result from Experiment #2 was plotted here. The C 1s spectrum can be deconvoluted into three peaks (dotted lines) by curve fitting. Their binding energies are 285.0, 286.6, and 288.7 eV, which can be attributed to C–C and C–H bonds, alcohol groups (C–OH), and carboxyl groups (–COOH), respectively.

significantly higher conversion rates of reduced carbon formation from more oxidized forms of dissolved carbon during Experiment #1, despite the relatively low H_2/CO_2 characterizing the experiment (Table 2 and Fig. 5). The approximately 50% greater conversion rate observed for Experiment #1 relative to Experiment #3, may result from enhanced catalytic effects of hydrocarbon intermediaries synthesized during the experiment, which may accumulate on the surface of magnetite, consistent with XPS data and mass balance constraints. Indeed, it is perhaps the combination of residual surface carbon phases/components with newly synthesized hydrocarbons on magnetite that enhance the catalytic effectiveness expressed by results of this experiment. The identity of the synthesized hydrocarbon intermediaries and mechanism by which they attach to the magnetite surface is uncertain, however, precluding unambiguous interpretation of the conversion rate data from each of the experiments.

4.2. Carbon and hydrogen isotope fractionations

The most significant feature of the hydrocarbon $\delta^{13}C$ results is the substantial depletion in $\delta^{13}C$ values of CH_4 over time in Experiments #1 and #3. The control Experiment 1c results show a steady state CO_2/CH_4 ratio over time, indicating that the changes in $\delta^{13}C$ values of CH_4 are not due to an increasing contribution of background carbon. Assuming that the background contribution of CH_4 stays steady at approximately 0.12 mmol/kg as suggested by the control Experiment 1c, we can test the assumption that the decrease in $\delta^{13}C$ of CH_4 in Experiment #1 over time is simply due to increasing CH_4 production by FTT (e.g. production of 0.27 mmol/kg CH_4 (0.39 − 0.12 mmol/kg) by FTT by 66 h and 0.51 mmol/kg CH_4 (0.63 − 0.12 mmol/kg) by FTT by 570 h). If the system is controlled by this simple two component mass balance, and knowing the measured $\delta^{13}C$ values for total CH_4 at 66 and 570 h are −36.1‰ and −46.3‰, respectively (Table 2), the following two equations can be solved to estimate X ($\delta^{13}C$ value for background CH_4) and Y ($\delta^{13}C$ value for FTT CH_4):

$$0.12X + 0.27Y = 0.39 \times (-36.1‰) \quad (1)$$

$$0.12X + 0.51Y = 0.63 \times (-46.3‰) \quad (2)$$

Based on this simple mass balance, the estimated FTT produced CH_4 end-member must have a $\delta^{13}C$ value of −62.9‰ and the background CH_4 a $\delta^{13}C$ value of approximately +24‰. Given that the $\delta^{13}C$ value for the surface carbon associated with untreated magnetite was −12.8‰ prior to reaction, and −28.8‰ following Experiment #1, such highly enriched values for the background CH_4 as +24‰ seem unlikely. The plausible explanation is that in fact the temporal depletion in $\delta^{13}C$ values of CH_4 is not entirely due to simple mixing of an increasing component of FTT produced CH_4 with background CH_4. For example, in Experiment #3, $\delta^{13}C$ value of CH_4 changed from −33.5‰ to −39.2‰, while its concentration kept relatively constant. In contrast to the temporal shifts in $\delta^{13}C$ of CH_4, $\delta^{13}C$ values for C_2H_6 and C_3H_8 show only slight enrichment of 1–2‰ over time. This may be consistent with not only production of CH_4 and higher hydrocarbons by FTT, but back reaction (depolymerization) of higher hydrocarbons to CH_4 over time, resulting in progressive ^{13}C depletion in CH_4 and ^{13}C enrichment in C_2H_6 and C_3H_8. It should be noted, however, that the total amount of enrichment in C_2H_6 and C_3H_8 is only slightly larger than analytical uncertainty (±0.5‰) and that $\delta^{13}C$ values for C_2H_6 and C_3H_8 should change more than that for CH_4 because of its much larger concentration compared to C_2H_6 and C_3H_8. Hence, another possible scenario is that the second mechanism is occurring, possibly reactions of the hydrocarbons with the produced surface carbon layer on magnetite, or unidentified

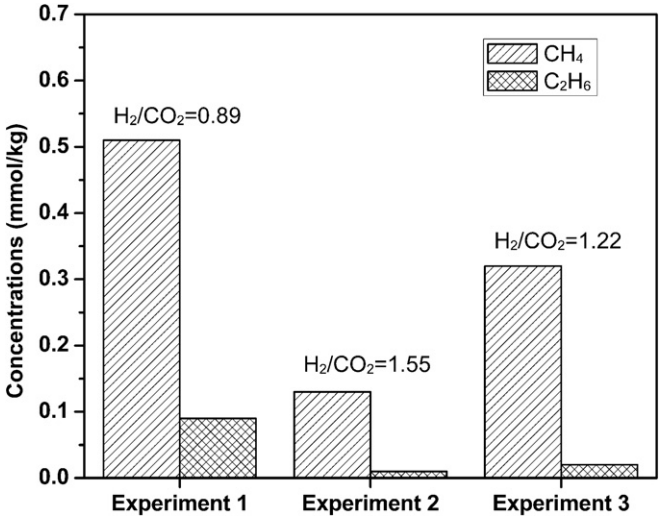

Fig. 5. Concentrations of produced CH_4 and C_2H_6 in all three hydrothermal experiments involving carbon reduction processes at 400 °C and 500 bars. For Experiment #1, the amount of CH_4 from decomposition of magnetite-derived surface carbon compounds is subtracted from the total produced CH_4. With carbon residue on magnetite surface, Experiment #1 has the highest amounts of CH_4 and C_2H_6 among three experiments, even with the lowest H_2/CO_2 ratio, suggesting the role of surface carbon residue as chain initiator to facilitate hydrocarbon formation.

aqueous hydrocarbons that affect CH_4 preferentially compared to C_2H_6 and C_3H_8. Since CH_4, C_2H_6 and C_3H_8 show similar results in both Experiment #1 (untreated magnetite) and Experiment #3 (treated magnetite) is it apparent that the mechanism is independent of the treatment or non-treatment of the mineral surface.

Carbon isotope values for dissolved reduced carbon species for which time-series data are available (Experiments #1 and #3) reflect non-equilibrium fractionation effects as well as mass balance constraints imposed by dissolution/decomposition, recrystallization, and FTT synthesis of solid and aqueous hydrocarbons. Three different reduced carbon components/phases are apparently involved: (1) dissolved CO and C_1–C_4 alkanes; (2) longer chain carbon-bearing species on magnetite surfaces; and, (3) presently unidentified aqueous hydrocarbon(s). Direct measurement of the chemical and isotopic composition of dissolved carbon species (reduced and oxidized), together with data for the abundance and carbon isotopic composition of magnetite-sourced carbon components before and following experiments, permit the average composition and carbon isotopic composition of the remaining dissolved hydrocarbon(s) to be estimated, as follows:

$$X_S\delta^{13}C_S + X_{S_1}\delta^{13}C_{S_1} = X_{CO_2}\delta^{13}C_{CO_2} + \sum X_{CO,C_1-C_4}\delta^{13}C_{CO,C_1-C_4} + X_{S_2}\delta^{13}C_{S_2} + X_A\delta^{13}C_A \quad (3)$$

Where subscript S, S_1, S_2 and A refer to carbon source (formic acid in Experiment #1, CO_2 in Experiments #2 and #3), surface carbon species before and after reaction, and unidentified aqueous hydrocarbon species, respectively. The X terms, which sum to unity on each side of the equation (left: before reaction; right: after reaction), are mole fractions of each of the carbon components. Solution of Eq. (3) indicates an average abundance (CO_2 equivalent concentration) and carbon isotopic composition of the bulk aqueous hydrocarbon of 24.7 mmol/kg and −18.2‰, 10.8 mmol/kg and −8.2‰, and 13.8 mmol/kg and −10.9‰ for Experiments #1, #2 and #3, respectively.

Overall, the unidentified aqueous hydrocarbons have the highest CO_2 equivalent concentration (Fig. 6) and $\delta^{13}C$ value among produced carbon-bearing species in each experiment. These unidentified aqueous hydrocarbons might include oxygenated compounds (for example, alcohols) and longer chain hydrocarbons with low absolute concentrations. Previous isotopic studies of FTT synthesis show that both short- and long-chain hydrocarbons are depleted in ^{13}C relative to CO_2 and CO (Lancet and Anders, 1970; Yuen et al., 1984; Hu et al., 1998; McCollom and Seewald, 2006). This contrasts with our results, but may be attributed to differences in experimental design and conditions (catalyst, bulk compositions, T and P), precluding unambiguous comparison. It is important to emphasize that the predicted concentration and carbon isotope composition of the putative aqueous hydrocarbon component is an average value and may actually represent the sum of a number of different species, the precise representation of which must await results of additional experiments that are presently in progress.

Recent studies suggest that abiotic formation of hydrocarbons produces carbon and hydrogen isotope signatures distinct from those produced by conventional biogenic (both microbial and thermogenic) processes (Sherwood Lollar et al., 2002; Onstott et al., 2006). Nonetheless, understanding the details of variation in carbon and hydrogen isotope signatures between abiogenically synthesized hydrocarbon compounds is still in its early stages. Sherwood Lollar et al. (2002, 2006) suggested that a trend of carbon isotope depletion but hydrogen isotope enrichment between CH_4 and C_2H_6 might be an indicator of abiogenic

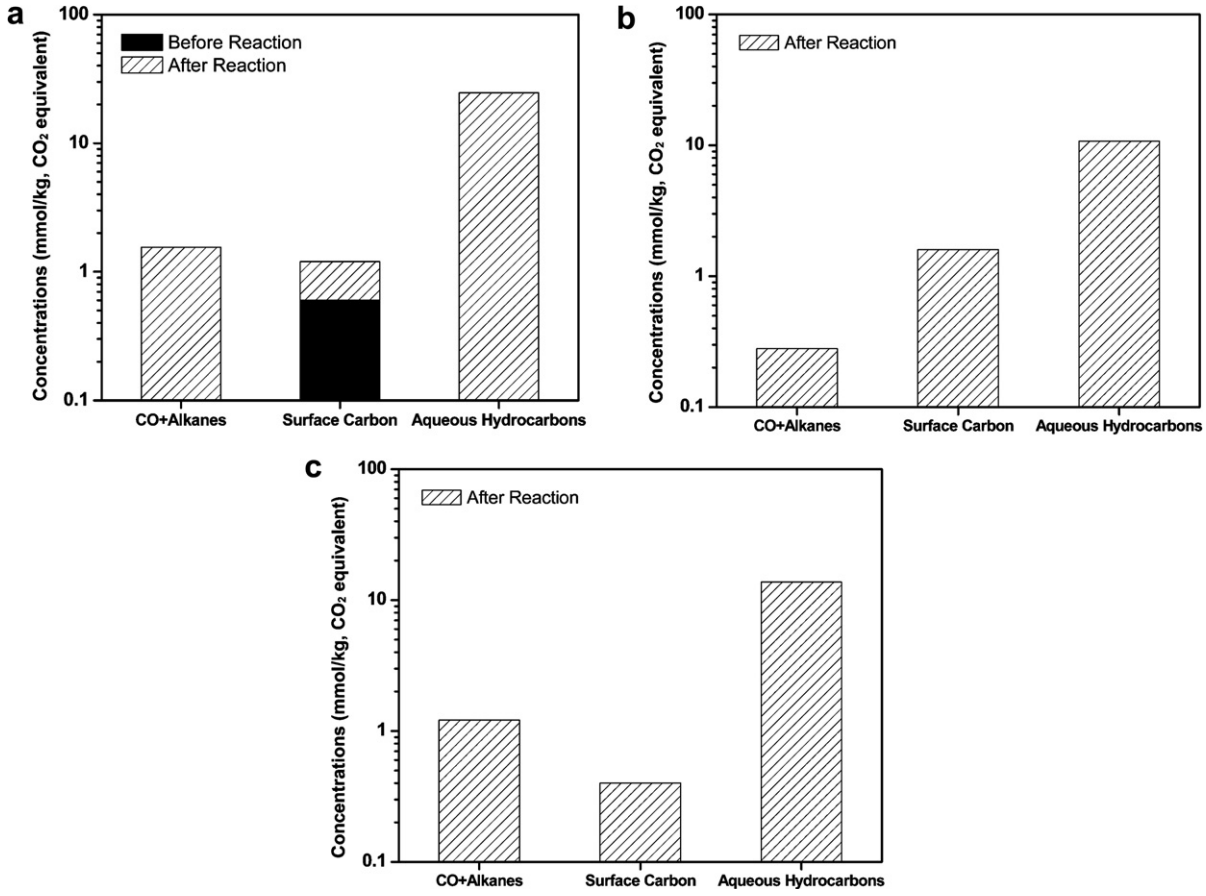

Fig. 6. Distribution of carbon-bearing components before and after Experiment #1 (a), after Experiment #2 (b) and #3 (c). These carbon-bearing components include dissolved CO and alkanes, longer chain carbon species on magnetite, and unidentified aqueous hydrocarbons. The concentration of unidentified aqueous hydrocarbons was calculated based on constraints imposed by carbon mass balance calculations (see text).

formation via polymerization reactions and called for more detailed integration of isotopic analysis and experimental research to decipher the specific patterns associated with abiogenic reaction mechanisms. The current study provides a methodology for such integration of compound specific isotope analysis with abiogenic synthesis experiments and reports the first values obtained for hydrogen as well as carbon isotope compositions in such experiments.

The experimentally derived carbon isotope data also provide support for the notion expressed in the literature (Horita and Berndt, 1999; Sherwood Lollar et al., 2002; Du et al., 2003; Huang et al., 2004) that "carbon isotope reversal" trends are not an unambiguous indicator of abiogenic gases. The carbon isotope data for CH_4, C_2H_6 and C_3H_8, especially with reaction progress, suggest a complex series of processes involving both FTT synthesis and depolymerization back to CH_4, and/or reaction with surface carbon layers related to the mineral surface and unidentified aqueous hydrocarbons. For example, the observed moderate increase in $\delta^{13}C$ values of abiotically formed alkanes with increasing carbon number (C_1–C_3) is consistent with depolymerization of the longer chain hydrocarbons that accumulate on the surface of magnetite. An explicit reaction mechanism involved in abiogenic hydrocarbon formation processes is still needed, however, to account unambiguously for observed carbon and hydrogen isotope fractionation and time-series changes in fluid chemistry.

4.3. Geologic and geochemical implications

The results of this study can be related in large part to complex reaction schemes under hydrothermal conditions, but also to the active, and in some cases, preferential participation of labile ^{12}C-bearing components in carbon reduction processes. The latter result is in general agreement with earlier data from experiments using labeled carbon sources (Foustoukos and Seyfried, 2004), which showed that ^{12}C from carbon sources chemisorbed on surfaces of mineral catalysts constitute a preferential hydrocarbon chain growth mechanism, as indicated by the abundance and mass of synthesized ethane and propane isotopomers. It is well known that carbon-bearing phases including hydrocarbons are often associated with mantle rocks (Tingle et al., 1990; Sugisaki and Mimura, 1994; Kenney et al., 2002; Scott et al., 2004), the composition and abundance of which may facilitate the formation and influence the isoto-

pic composition of other dissolved hydrocarbons (as occurred during the present study, especially Experiment #1), assuming these rocks undergo hydrothermal alteration under an appropriate set of physical and chemical conditions.

The likelihood of multiple carbon sources, together with complex chain growth processes, however, can obscure the origin and evolution of hydrocarbons in hydrothermal vent fluids. For example, recent radiocarbon isotope data for dissolved hydrocarbons in vent fluids issuing from the ultramafic-hosted Lost City system suggest that the carbon source for vent fluid hydrocarbons is host-rock derived (Proskurowski et al., 2005), offering the possibility of involvement of many of the processes outlined above as subseafloor carbon reduction reactions proceed. Moreover, the presence of C_{16}–C_{29} linear saturated hydrocarbons accompanied by abundant CH_4 (2.2 mmol/kg) dissolved in vent fluids issuing from the high-temperature Rainbow hydrothermal system (36°N, MAR) (Holm and Charlou, 2001; Charlou et al., 2002, 2005), might also suggest host-rock carbon sources participating in and perhaps facilitating complex FTT synthesis reactions, qualitatively and quantitatively analogous to those recognized during the present investigation. In particular, time-series data for high-temperature vent fluids at Rainbow indicate decreasing $\delta^{13}C$ values of CH_4 (-15.8 to $-18.2‰$), while $\delta^{13}C$ of CO_2 remains constant ($-3.1‰$) (Charlou et al., 2002). This is consistent with our experimental observation, which could involve the separation of increasingly greater fractions of CH_4 from coexisting abiotically produced long-chain surface hydrocarbons. Further clues to the existence of such processes may be found in the concentration and isotopic composition of the complex hydrocarbons reported for the Rainbow vent fluids, although data are not yet available for the isotopic composition of these and other hydrocarbon species at Rainbow, precluding more rigorous testing of experimental predictions.

Field observation from hydrothermal vent and geothermal systems often indicate that H_2O, H_2, and CH_4 are in H isotope equilibrium at temperatures above 200 °C (Welhan and Craig, 1983; Lyon and Hulston, 1984; Horibe and Craig, 1995). Recent study of Lost City hydrothermal system (Proskurowski et al., 2006) also shows that dissolved H_2 is in H isotopic equilibrium with H_2O and CH_4 at temperatures ranging from approximately 50 to 130 °C. Hydrogen isotope equilibrium in the H_2O–H_2–CH_4 system, however, is not completely observed during our experiments, relatively long reaction times and high-temperature notwithstanding. This likely results from the still uncertain role of the metastable existence of the proposed long-chain hydrocarbons on rates and mechanisms of chemical and isotope exchange. On the other hand, the mechanism that seems to enhance rates of H isotope exchange between H_2, H_2O and CH_4 in natural hydrothermal systems, such as at Lost City (as indicated by the correspondence between measured and isotopically calculated vent fluid temperatures), is also uncertain. Possibly, this may involve the existence of unusually effective mineral catalysts along the fluid flow path and/or relatively long residence times in the crust facilitating chemical and isotope exchange. Clearly, to fully understand the mechanism and kinetics of H isotope exchange during abiotic hydrocarbon formation under hydrothermal conditions, further studies involving compositionally variable mineral catalysts at a wide range of temperatures and pressures are necessary.

5. CONCLUSIONS

Hydrothermal experiments designed to investigate carbon reduction processes were performed at 400 °C and 500 bars to understand better the origin and evolution of reduced carbon species in subseafloor hydrothermal systems. Magnetite, a mineral common to ultramafic-hosted hydrothermal systems at mid-ocean ridges, served as a catalyst for carbon reduction reactions in H_2 and CO_2-bearing aqueous fluids. Two different experimental strategies were used to achieve relatively high dissolved H_2 and CO_2 concentrations. The first entailed decarboxylation of formic acid, while the second involved direct injection of CO_2 into the reaction cell, which was then followed by H_2-injection, ultimately achieving appropriate dissolved concentrations and unique H_2/CO_2 ratios. The magnetite that was used in experiments with the decarboxylation products of formic acid was not pretreated in any way, and therefore, contained modest amounts of "background" carbon introduced during mineral processing. All other experiments, however, involved magnetite that was pretreated, in which these compounds were quantitatively removed prior to reaction with the variably reducing and CO_2-rich fluids. Prior to all experiments, the abundance and isotope composition of all carbon components (aqueous and solid forms) were determined to better constrain reaction processes.

Dissolved CO and C_1–C_3 hydrocarbons were observed in fluids from all experiments. In keeping with previous experimental data, dissolved CO_2 and CO concentrations were consistent with constraints imposed by chemical equilibrium in the H_2-bearing fluids. Although this was not the case for dissolved hydrocarbons, data indicate that increases in H_2/CO_2 ratio of the fluid resulted in corresponding increases in dissolved alkanes, confirming a cause and effect relationship. Unusually, high CH_4 concentrations, however, were observed in the experiment involving non-pretreated magnetite. Although part of this can be accounted for by simple decomposition of the background carbon-bearing phase(s), it is more likely that the combination of these effects with more abundant hydrocarbons synthesized by FTT processes (revealed by non-conservative behavior of dissolved CO_2 and H_2 recognized during all experiments), may have introduced other catalytic schemes affecting abiotic formation of hydrocarbons, both qualitatively and quantitatively.

H isotopic equilibrium has been reached for H_2O–H_2, while partial equilibration for H_2O–CH_4 and CH_4–H_2 may have been attained. No "isotopic reversal" trend was observed for ^{13}C values of alkanes with increasing carbon number, suggesting that carbon isotope systematics during abiotic hydrocarbon formation may be a sensitive function of specific chain growth mechanism. In aqueous fluids at elevated temperatures and pressures, a complex mechanism involving formation of long chain hydrocarbons on

magnetite surfaces, followed by depolymerization and/or reaction with other hydrocarbons, is required to account for time-series changes in the concentration and carbon isotopic composition of dissolved carbon species during the experiments.

It is becoming increasingly clear that the abundance and distribution of dissolved hydrocarbons in vent fluids issuing from ultramafic-hosted hydrothermal systems represent the end result of a series of reactions that likely include multiple carbon sources coexisting with minerals, which may fundamentally affect abiotic pathways. Clearly, much remains to be learned of the combined effects of carbon reduction schemes in the presence of multiple carbon-bearing components in rocks containing catalytically active minerals and coexisting reducing fluids at elevated temperatures and pressures—a goal best realized by the integration of experimental, field and theoretically based investigations.

ACKNOWLEDGMENTS

We thank Rick Haasch at the Center for Microanalysis of Materials, University of Illinois for invaluable assistance in XPS analysis. We would also like to thank Dionysios Foustoukos for his helpful suggestions and discussion. Research support from NSF Grant OCE-0549457 and the American Chemical Society, Petroleum Research Fund PRF-41885-AC2 are gratefully acknowledged. Support for the isotopic analyses is provided through the Canadian Space Agency, NASA Astrobiology Institute IPTAI team, with additional funds to Barbara Sherwood Lollar from NSERC and the Canada Council Killam Fellowship. Research of J. Horita was sponsored by the Division of Chemical Sciences, Geosciences, and Biosciences, Office of Basic Energy Sciences, U.S. Department of Energy, under contract DE-AC05-00OR22725, Oak Ridge National Laboratory, managed by UT-Battelle, LLC. Helpful comments by Associate Editor Jeff Alt, J. L. Charlou, and two anonymous reviewers are appreciated.

REFERENCES

Alt J. C., and Shanks, III, W. C. (2003) Serpentinization of abyssal peridotites from the MARK area, Mid-Atlantic Ridge: sulfur geochemistry and reaction modeling. *Geochim. Cosmochim. Acta* **67**(4), 641–653.

Anderson R. B. (1984a) *The Fischer–Tropsch Synthesis*. Academic Press, New York.

Anderson R. B. (1984b) Forty years with the Fischer–Tropsch synthesis 1944–1984. *Stud. Sur. Sci. Catal.* **19**, 457–461.

Aharon P. (1994) Geology and biology of modern and ancient submarine hydrocarbon seeps and vents: an introduction. *Geo-Mar. Lett.* **14**(1), 69–73.

Baross J. A., Wilcock W. S. D., Kelley D. S., DeLong E. F., and Cary S. C. (2004) The subsurface biosphere at mid-ocean ridges: issues and challenges. In *The Subseafloor Biosphere at Mid-Ocean Ridges* (eds. W.S. D. Wilcock, E.F. DeLong, D.S. Kelley, J.A. Baross and S.C. Cary). Geophysical Monograph 144. American Geophysical Union, Washington DC, pp. 1–11.

Bell A. T. (1986) The mechanism of the Fischer–Tropsch Synthesis. In *Heterogeneous Catalysis*. Texas A & M University Press, College Station, TX.

Berndt M., Allen D., and Seyfried, Jr., W. E. (1996) Reduction of CO_2 during serpentinization of olivine at 300 °C and 500 bar. *Geology* **24**, 351–354.

Bethke C. M. (1996) *Geochemical Reaction Modeling*. Oxford University Press, New York.

Chang S., Des Marais D., Mack R., Miller S. L., and Strathearn G. E. (1983) Prebiotic organic synthesis and the origin of life. In *Earth's Earliest Biosphere, its Origin and Evolution* (ed. J.W. Schopf). Princeton University Press, Princeton, NJ, pp. 54–92.

Charlou J. L., and Donval J. P. (1993) Hydrothermal methane venting between 12°N and 26°N along the Mid-Atlantic Ridge. *J. Geophys. Res. [Solid Earth]* **98**(B6), 9625–9642.

Charlou J. L., Donval J. P., Douville E., Radford-Knoery J., Fouquet Y., Bougault H., Jean-Baptiste P., Stievenard M., German C., and FLORES Cruise Scientific Party (1997) High methane flux between 15°N and the Azores triple junction, Mid-Atlantic Ridge: hydrothermal and serpentinization processes. *Eos Trans. Am. Geophys. Union* **78**(46), 83.

Charlou J. L., Fouquet Y., Bougault H., Donval J. P., Etoubleau P., Jean-Baptiste P., Dapoigny A., Appriou P., and Rona P. A. (1998) Intense CH_4 plumes generated by serpentinization of ultramafic rocks at the intersection of the 15°20′N fracture zone and the Mid-Atlantic Ridge. *Geochim. Cosmochim. Acta* **62**(13), 2323–2333.

Charlou J. L., Donval J. P., Fouquet Y., Jean-Baptiste P., and Holm N. (2002) Geochemistry of high H_2 and CH_4 vent fluids issuing from ultramafic rocks at the rainbow hydrothermal field (36°14′N, MAR). *Chem. Geol.* **191**, 345–359.

Charlou J., Donval J., Fouquet Y., Jean-Baptiste P., Dehairs F., Holm N., and Godfroy A. (2005) Organics in hydrothermal fluids from ultramafics on the Mid-Atlantic Ridge (MAR)—abiogenic and/or biogenic origin? Eos Trans. American Geophysical Union 86(52), Fall Meet. Suppl., Abstract B23D-08.

Chung H. M., Gormly J. R., and Squires R. M. (1988) Origin of gaseous hydrocarbons in subsurface environments: theoretical considerations of carbon isotope distribution. *Chem. Geol.* **71**(1–3), 97–104.

Deming J. W., and Baross J. A. (1993) Deep-sea smokers: windows to a subsurface biosphere. *Geochim. Cosmochim. Acta* **57**, 3219–3230.

Des Marais D. J., Donchin J. H., Nehring N. L., and Truesdell A. (1981) Molecular carbon isotopic evidence for the origin of geothermal hydrocarbons. *Nature* **292**, 826–828.

Douville E., Charlou J. L., Oelkers E. H., Bienvenu P., Jove Colon C. F., Donval J. P., Fouquet Y., Prieur D., and Appriou P. (2002) The rainbow vent fluids (36°14′N, MAR): the influence of ultramafic rocks and phase separation on trace metal content in Mid-Atlantic Ridge hydrothermal fluids. *Chem. Geol.* **184**, 37–48.

Du J., Jin Z., Xie H., Bai L., and Liu W. (2003) Stable carbon isotope compositions of gaseous hydrocarbons produced from high pressure and high temperature pyrolysis of lignite. *Org. Geochem.* **34**, 97–104.

Fischer F., and Tropsch H. (1926) Die Erodölsynthese bei gewöhnlichem druck aus den vergangsprodukten der kohlen. *Brennstoff-Chemie* **7**, 97–116.

Foustoukos D., and Seyfried, Jr., W. E. (2004) Hydrocarbons in hydrothermal vent fluids: the role of chromium-bearing catalysts. *Science* **304**, 1002–1005.

Galimov E. M. (1975) *Carbon Isotopes In Oil–Gas Geology. NASA TT F-682. Translated from Izotopy ugleroda v neftegazovoy geologii*. Nedra Press, Moscow.

Holm N. G., and Charlou J. L. (2001) Initial indications of abiotic formation of hydrocarbons in the rainbow ultramafic hydrothermal system, Mid-Atlantic ridge. *Earth Planet. Sci. Lett.* **191**(1–2), 1–8.

Horibe Y., and Craig H. (1995) D/H fractionation in the system methane–hydrogen–water. *Geochim. Cosmochim. Acta* **59**(24), 5209–5217.

Horita J. (2001) Carbon isotope exchange in the system CO_2–CH_4 at elevated temperatures. *Geochim. Cosmochim. Acta* **65**, 1907–1919.

Horita J. (2005) Some perspectives on isotope biosignatures for early life. *Chem. Geol.* **218**, 171–186.

Horita J., and Berndt M. E. (1999) Abiogenic methane formation and isotopic fractionation under hydrothermal conditions. *Science* **285**, 1055–1057.

Horita J. and Cole D. R. (2004) Stable isotope partitioning in aqueous and hydrothermal systems to elevated temperatures. In *Aqueous Systems at Elevated Temperatures and Pressures: Physical Chemistry in Water, Steam and Hydrothermal Solutions* (eds. D.A. Palmer, R. Fernández-Prini and A.H. Harvey). Academic Press, pp. 277–319.

Hu G., Ouyang Z., Wang X., and Wen Q. (1998) Carbon isotopic fractionation in the process of Fischer–Tropsch reaction in primitive solar nebula. *Sci. China* **41**, 202–207.

Huang H., Yang J., Yang Y., and Du X. (2004) Geochemistry of natural gases in deep strata of the Songliao Basin, NE China. *Coal Geol.* **58**, 231–244.

James A. T. (1983) Correlation of natural gas by use of carbon isotopic distribution between hydrocarbon components. *Am. Assoc. Petrol. Geol. Bull.* **67**(7), 1176–1191.

Janecky D. R., and Seyfried, Jr., W. E. (1986) Hydrothermal serpentinization of peridotite within the oceanic crust: experimental investigations of mineralogy and major element chemistry. *Geochim. Cosmochim. Acta* **50**, 1357–1378.

Jenden P. D., Hilton D. R., Kaplan I. R., and Craig H. (1993) Abiogenic hydrocarbons and mantle helium in oil and gas fields. In *The Future of Energy Gases* (eds. D. G. Howell, K. Wiese, M. Fanelli, L.L. Zink, F. Cole) (US Geological Survey Professional Paper 1570), pp. 31–56.

Johnson J. W., Oelkers E. H., and Helgeson H. C. (1992) SUPCRT92—a software package for calculating the standard molal thermodynamic properties of minerals, gases, aqueous species, and reactions from 1 bar to 5000 bar and 0 to 1000 °C. *Comput. Geosci.* **18**(7), 899–947.

Karl D. M. (1995) *The Microbiology of Deep-Sea Hydrothermal Vents*. CRC Press, Boca Raton, New York.

Karl D. M., Wirsen C. O., and Jannasch H. W. (1980) Deep-sea primary production at the Galapagos hydrothermal vents. *Science* **207**(4437), 1345–1347.

Kelley D. S. (1996) Methane-rich fluids in the oceanic crust. *J. Geophys. Res. [Solid Earth]* **101**(B2), 2943–2962.

Kelley D. S., and Früh-Green G. L. (1999) Abiogenic methane in deep-seated mid-ocean ridge environments: insights from stable isotope analyses. *J. Geophys. Res. [Solid Earth]* **104**(B5), 10439–10460.

Kelley D. S., Baross J. A., and Delaney J. R. (2002) Volcanoes, fluids and life at mid-ocean ridge spreading centers. *Ann. Rev. Earth Planet. Sci.* **30**, 385–491.

Kelley D. S., Lilley M. D., and Früh-Green G. L. (2004) Volatiles in submarine environments: food for life. In *The Subseafloor Biosphere at Mid-Ocean Ridges* (eds. W.S.D. Wilcock, E.F. DeLong, D.S. Kelley, J.A. Baross and S.C. Cary). Geophysical Monograph 144. American Geophysical Union, Washington DC, pp. 167–189.

Kenney J. F., Kutcherov V. A., Bendeliani N. A., and Alekseev V. A. (2002) The evolution of multicomponent systems at high pressures: VI. The thermodynamic stability of the hydrogen–carbon system: the genesis of hydrocarbons and the origin of petroleum. *Proc. Natl. Acad. Sci. USA* **99**(17), 10976–10981.

Kugler E. L. and Steffgen F. W. (1979) *Hydrocarbon Synthesis from Carbon Monoxide and Hydrogen*. American Chemical Society, Advances in Chemistry Series 178, Washington, DC.

Lancet H. S., and Anders E. (1970) Carbon isotope fractionation in the Fischer–Tropsch synthesis of methane. *Science* **170**, 980–982.

Lyon G. L., and Hulston J. R. (1984) Carbon and hydrogen isotopic compositions of New Zealand geothermal gases. *Geochim. Cosmochim. Acta* **48**(6), 1161–1171.

McCollom T. M., and Seewald J. S. (2001) A reassessment of the potential for reduction of dissolved CO_2 to hydrocarbons during serpentinization of olivine. *Geochim. Cosmochim. Acta* **65**, 3769–3778.

McCollom T. M., and Seewald J. S. (2003) Experimental constraints on the hydrothermal reactivity of organic acids and acid anions: I. Formic acid and formate. *Geochim. Cosmochim. Acta* **67**(19), 3625–3644.

McCollom T. M., and Seewald J. S. (2006) Carbon isotope composition of organic compounds produced by abiotic synthesis under hydrothermal conditions. *Earth Planet. Sci. Lett.* **243**(1–2), 74–84.

Onstott T., Lin L.-H., Davidson M., Mislowack B., Borcsik M., Hall J., Slater G., Ward J., Sherwood Lollar B., Lippmann-Pipke J., Boice E., Pratt L., Pfiffner S., Moser D., Gihring T., Kieft T., Phelps T., Vanheerden E., Litthaur D., Deflaun M., Rothmel R., Wanger G., and Southam G. (2006) The origin and age of biogeochemical trends in deep fracture water of the Witwatersrand Basin, South Africa. *Geomicrobiol. J.* **23**(6), 369–414.

Oremland R. S., and Des Marais D. J. (1983) Distribution, abundance and carbon isotopic composition of gaseous hydrocarbons in Big Soda Lake, Nevada: an alkaline, meromictic lake. *Geochim. Cosmochim. Acta* **47**, 2107–2114.

Proskurowski G., Lilley M., Olson E., Kelley D., and Frueh-Green G. (2005) *Low Molecular Weight Hydrocarbon Production at the Lost City Hydrothermal Field. Eos Trans.*, American Geophysical Union 86(52), Fall Meet. Suppl., Abstract V51B-1485.

Proskurowski G., Lilley M., Kelley D., and Olson E. (2006) Low temperature volatile production at the Lost City hydrothermal field, evidence from a hydrogen stable isotope geothermometer. *Chem. Geol.* **229**(4), 331–343.

Richet P., Bottinga Y., and Javoy M. (1977) A review of hydrogen, carbon, nitrogen, oxygen, sulphur, and chlorine stable isotope fractionation among gaseous molecules. *Ann. Rev. Earth Planet. Sci.* **5**, 65–110.

Sackett W. M. (1978) Carbon and hydrogen isotope effects during the thermocatalytic production of hydrocarbons in laboratory simulation experiments. *Geochim. Cosmochim. Acta* **42**(6), 571–580.

Schoell M. (1983) Genetic characterization of natural gases. *Am. Assoc. Petrol. Geol. Bull.* **67**, 2225–2238.

Scott H. P., Hemley R. J., Mao H., Herschbach D. R., Fried L. E., Howard W. M., and Bastea S. (2004) Generation of methane in the earth's mantle: in situ high pressure–temperature measurements of carbonate reduction. *Proc. Natl. Acad. Sci. USA* **101**(39), 14023–14026.

Seewald J. S., Zolotov M. Y., and McCollom T. (2006) Experimental investigation of single carbon compounds under hydrothermal conditions. *Geochim. Cosmochim. Acta* **70**(2), 446–460.

Seyfried W. E. Jr, Janecky D. R., and Berndt M. E. (1987) Rocking autoclaves for hydrothermal experiments, II. The flexible reaction-cell system. In *Hydrothermal Experimental Techniques* (eds. G.C. Ulmer and H.L. Barnes). John Wiley and Sons, pp. 216–239.

Seyfried W. E. Jr., Foustoukos D. I., and Allen D. E. (2004) Ultramafic-hosted hydrothermal systems at mid-ocean ridges: Chemical and Physical controls on pH, redox, and carbon reduction reactions. In *Mid-Ocean Ridges: Hydrothermal Interactions between the Lithosphere and Oceans* (eds. C.R.

German, J. Lin, and L.M. Parson). Geophysical Monography 148. American Geophysical Union, pp. 267–284.

Sherwood Lollar B., Westgate T. D., Ward J. A., Slater G. F., and Lacrampe-Couloume G. (2002) Abiogenic formation of alkanes in the earth's crust as a minor source for global hydrocarbon reservoirs. *Nature* **416**, 522–524.

Sherwood Lollar B., Lacrampe-Couloume G., Slater G. F., Ward D. P., Moser D. P., Gihring T. M., Lin L.-H., and Onstott T. C. (2006) Unravelling abiogenic and biogenic sources of methane in the earth's deep subsurface. *Chem. Geol.* **226**(3–4), 328–339.

Shock E. L., Sassani C., Willis M., and Sverjensky D. A. (1997) Inorganic species in geologic fluids: correlations among standard molal thermodynamic properties of aqueous ions and hydroxide complexes. *Geochim. Cosmochim. Acta* **61**, 907–950.

Sugisaki R., and Mimura K. (1994) Mantle hydrocarbons: Abiotic or biotic? *Geochim. Cosmochim. Acta* **58**, 2527–2542.

Sverjensky D. A., Shock E. L., and Helgeson H. C. (1997) Prediction of the thermodynamic properties of aqueous metal complexes to 1000 °C and 5 kb. *Geochim. Cosmochim. Acta* **61**, 1359–1412.

Tingle T. N., Hochella, Jr., M. F., Becker C. H., and Malhorta R. (1990) Organic compounds on crack surfaces in olivine from San Carlos, Arizona and Hualalai Volcano, Hawaii. *Geochim. Cosmochim. Acta* **54**, 477–485.

Yu J., and Savage P. E. (1998) Decomposition of formic acid under hydrothermal conditions. *Ind. Eng. Chem. Res.* **37**, 2–10.

Yuen G. U., Blair N., Des Marais D. J., and Chang S. (1984) Carbon isotopic composition of low molecular weight hydrocarbons and monocarboxylic acids from Murchison meteorite. *Nature* **307**, 252–254.

Yuen G. U., Pecore J. A., Kerridge J. F., Pinnavaia T. J., Rightor E. G., and Flores J. (1990) Carbon isotopic fractionation in Fischer–Tropsch type reactions. *Lunar Planet. Sci. Conf.* **XXI**, 1367–1368.

Waples D. W., and Tornheim L. (1978) Mathematical models for petroleum-forming processes: carbon isotope fractionation. *Geochim. Cosmochim. Acta* **42**(5), 467–472.

Ward J. A. (2002) *Identifying Subsurface Gas Origins: Within the Witwatersrand Basin, South Africa*. Masters of Science Thesis, University of Toronto.

Ward J., Slater G. F., Moser D., Lin L., Lacrampe-Couloume G., Bonin A. S., Davidson M., Hall J. A., Mislowack B., Bellamy R. E. S., Onstott T. C., and Sherwood Lollar B. (2004) Microbial hydrocarbon gases in the Witwatersrand Basin, South Africa: implications for the deep biosphere. *Geochim. Cosmochim. Acta* **68**(15), 3239–3250.

Welhan J. A. (1988) Origins of methane in hydrothermal systems. *Chem. Geol.* **71**(1–3), 183–198.

Welhan J. A. and Craig H. (1983) Methane, hydrogen and helium in hydrothermal fluids at 21°N on the East Pacific Rise. In *Hydrothermal Processes at Seafloor Spreading Centers* (eds. P.A. Rona, K. Bostroem, L. Laubier, K.L. Smith Jr.). Plenum Press, New York, NY, United States, pp. 391–409.

Wolery T. J. and Daveler S. A. (1992) *EQ6, a Computer Program for Reaction Path Modeling of Aqueous Geochemical Systems: Theoretical Manual, user's guide, and related Documentation (version 7.0) UCRL-MA-1 10662 PT IV*, Lawrence Livermore National Laboratory, Livermore, CA, 337 pp.

Associate editor: Jeffrey C. Alt